PHYSICAL REVIEW A **103**, 032818 (2021)

Isotope shifts in the metastable a^5F and excited y^5G^o terms of atomic titanium

Andrew O. Neely,[1,2,*] Kayleigh Cassella,[1,3] Scott Eustice,[1,2] and Dan M. Stamper-Kurn[1,2,4,†]
[1]*Department of Physics, University of California, Berkeley, Berkeley, California 94720, USA*
[2]*Challenge Institute for Quantum Computation, University of California, Berkeley, California 94709, USA*
[3]*Atom Computing Inc., Berkeley, California 94710, USA*
[4]*Materials Science Division, Lawrence Berkeley National Laboratory, Berkeley, California 94720, USA*

(Received 12 November 2020; accepted 25 February 2021; published 15 March 2021)

We measure and analyze the isotope shifts in the multiplet of transitions between the metastable a^5F and excited y^5G^o terms of neutral titanium by probing a titanium vapor in a hollow cathode lamp using saturated absorption spectroscopy. We resolve the five $J \rightarrow J+1$ and the four $J \rightarrow J$ transitions within the multiplet for each of the three $I = 0$ stable isotopes (^{46}Ti, ^{48}Ti, and ^{50}Ti). The isotope shifts on these transitions allow us to determine the isotope-dependent variation in the fine-structure splitting of the a^5F and y^5G^o levels themselves. Combined with existing knowledge of the nuclear charge radii of titanium nuclei, we derive the specific mass and field shifts, which arise from correlated electronic motion and electronic density at the nucleus respectively, and further observe a strong J-dependent variation in each. Our results yield insight into the electronic and nuclear structure of transition metal atoms like titanium and also characterize optical transitions that may allow for optical manipulation of ultracold gases of transition-metal species.

DOI: 10.1103/PhysRevA.103.032818

I. INTRODUCTION

The isotope shifts of atomic spectra encode information about the nuclear and electronic structure of the atom [1]. The dominant sources of these shifts are the normal mass shift, which occurs from a change in the system's reduced mass, the specific mass shift, which reflects correlations within the electronic wave function, and the field shift, which stems from changes in nuclear volume. As such, precise isotope shift measurements provide strong tests of atomic and nuclear structure theory [2–7]. A more precise examination of isotope shifts is also proposed as a means to reveal electron-nucleus interactions beyond those within the standard model [8,9]. Aside from probing atomic structure, isotope shifts also provide necessary information for isotope-specific laser cooling of titanium gases [10] and the interpretation of astrophysical spectra [11,12].

Transition-metal atoms provide compelling targets for isotope-shift investigations because of their intermediate complexity. Compared with alkali and alkali-earth-metal atoms, transition metals provide the additional richness of having partially filled d subshells. These generate multiple same-parity atomic states that are admixed by electron-electron interactions so as to yield large electron-electron correlations, which can be probed via the specific mass shift. The d subshell also shields the nuclear charge, thereby influencing the electronic charge density at the nucleus, and therefore is evident in measurements of the field shift. At the same time, transition metals are less complex than heavier elements such as lanthanides and actinides and are thus more amenable to theoretical descriptions.

Among the transition metals, titanium is a particularly attractive choice for such isotopic characterization [13–20]. Compared with heavier transition metals, titanium's smaller atomic number reduces the strength of relativistic effects and makes detailed atomic theory more tractable. Compared to other light transition metals, the large isotopic selection of titanium enriches the measurement of isotope shifts richer. Titanium's four valence electrons provide a rich complexity that is still accessible by theoretical techniques, and the near-degeneracy of the $3d$ and $4s$ levels adds to this [18]. Titanium has also been targeted for its tightly packed atomic level structure, which leads to many states marked by significant state mixing [18,20]. Titanium has also played an important role in nuclear physics, because its proximity to the magic proton number of $Z = 20$ and ^{50}Ti's magic neutron number of $N = 28$ results in a trend of decreasing nuclear size for increasing nucleon number [20–22]. Additionally, atomic titanium has recently been identified as a candidate for laser cooling [10]. Isotope shift investigations may therefore provide key information toward generating a new family of quantum degenerate atomic gases.

Here, we apply Doppler-free spectroscopy to resolve optical transitions of the three zero-nuclear-spin isotopes of titanium (^{46}Ti, ^{48}Ti, and ^{50}Ti; see Table I) and measure the isotope shifts on the multiplet of transitions between the a^5F and y^5G^o terms of atomic titanium, as shown in Fig. 1. The measured shifts on both the $J \rightarrow J$ and $J \rightarrow J+1$ transitions allow us to determine the J dependence of the isotopic variation of the fine structure splitting of both the a^5F and y^5G^o terms. Similar studies have focused on J-dependent isotope shift, noting effects from three distinct sources:

---

[*] neelya@berkeley.edu
[†] dmsk@berkeley.edu

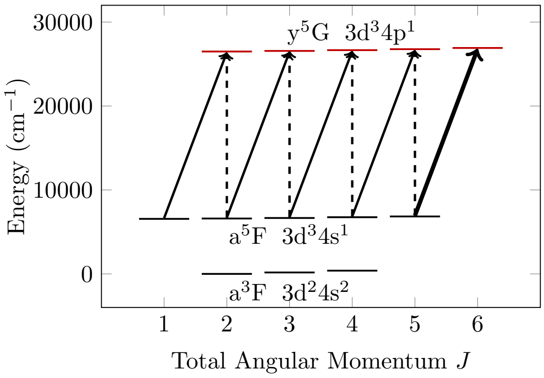

FIG. 1. The relevant energy levels in titanium. The a^5F_5 metastable state supports a near-cycling transition (bolded) to the $y^5G_6^o$ state. The $J \to J+1$ transitions (solid) and $J \to J$ transitions (dashed) together can be used to determine the level shifts of all of the levels in the a^5F_J and $y^5G_J^o$ manifolds. Black levels are even parity, and red (upper) levels are odd parity.

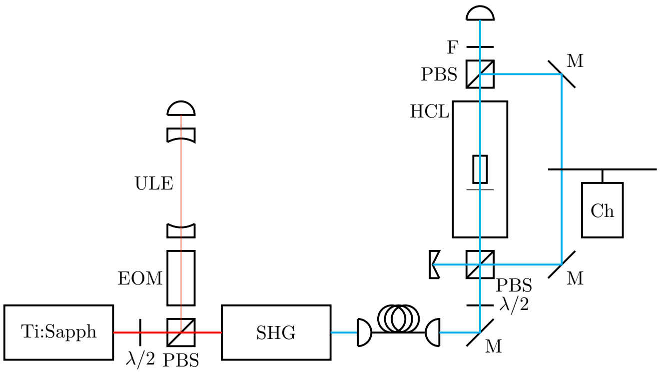

FIG. 2. The optical system. Infrared light is first generated with the Ti:sapph. Part of the light is sent through an electro-optic modulator (EOM) to an ultralow expansion cavity (ULE) for frequency referencing, and the rest of it is sent to the SHG stage. The frequency-doubled light is split into pump and probe beams, which counterpropagate through a hollow cathode lamp. A chopper (Ch) amplitude modulates the pump beam. A filtered photodiode detects the probe beam. Key: M, mirror; $\lambda/2$, half-wave plate; PBS, polarizing beam splitter; and F, filter.

spin-other-orbit (SOO), relativistic, and crossed-second-order (CSO) interactions [18,20,23]. The two energy terms studied here are largely free of admixture and therefore from the complication for CSO terms in the isotope shift, allowing for a cleaner measurement of J dependence due to SOO and relativistic interactions. These two terms also have larger ranges of J than those terms studied previously [18,20], allowing us to characterize the J dependence of isotope shifts more clearly.

We observe clear J-dependent variations of the isotope shift and interpret these variations as reflecting the J dependencies of electronic correlations and electron density in titanium. Among the measured transitions is the $a^5F_5 \to y^5G_6^o$ transition that has been identified as a near-cycling transition suited for laser cooling of titanium [10]. The measured isotope shifts on this line thereby provide key information for future efforts to laser cool the three bosonic isotopes of titanium.

II. EXPERIMENTAL SYSTEM

The a^5F term lies at an energy of about 6800 cm^{-1} above the ground a^3F term of titanium. In order to generate a population of metastable atoms, we use a hollow cathode lamp (HCL) (see Refs. [24,25] for other recent examples of HCL-based atomic spectroscopy), where titanium atoms are sputtered off a titanium cathode bombarded by Ne$^+$ ions. This titanium vapor contains a sufficient steady-state population of atoms in the a^5F levels to yield an optical density of around 10^{-3} for light resonant with the strongest transitions probed, namely the $a^5F_5 \to y^5G_6^o$ transition of the most abundant isotope, ^{48}Ti.

Laser spectroscopy was performed using the setup presented in Fig. 2. A Ti:sapphire laser [26] (Ti:sapph), whose emission wavelength was tuned between 996 and 1006 nm, was coupled to a resonant-cavity second-order harmonic generator (SHG). The fundamental laser frequency was scanned by actuating the length of the Ti:sapph cavity. The scanned laser frequency was calibrated by sampling the infrared fundamental light and detecting its transmission through the TEM$_{00}$ modes of an ultralow expansion (ULE) optical cavity [27]. The ULE cavity provides only sparse frequency markers spaced by the 1.5-GHz free spectral range of the cavity. Additional frequency markers were obtained by adding fixed-frequency sidebands to the light using a broadband electro-optic modulator, resulting in a denser calibration scale for the optical frequency, as seen in Fig. 3.

The Doppler-broadened single-beam absorption line width of about 1.4 GHz observed in the HCL on the transitions

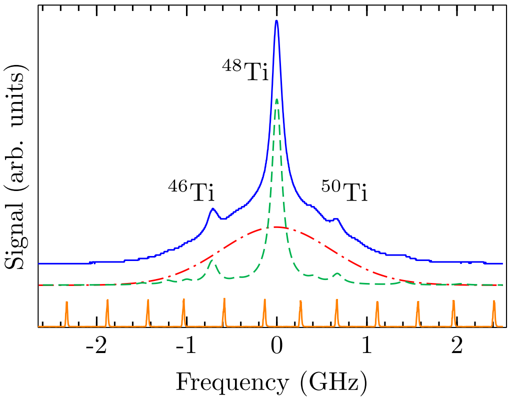

FIG. 3. Saturated absorption spectrum of the $a^5F_5 \to y^5G_6^o$ transition in titanium. The signal (blue, upper) obtained following demodulation at the chopping frequency shows clear peaks for the three $I = 0$ isotopes: ^{46}Ti, ^{48}Ti, and ^{50}Ti. The peak frequencies are obtained by fitting the observed spectrum as 10 Lorentzians (green, dashed) on top of the Gaussian background (red, dot-dashed) that is produced by diffusion of the excited-state atoms (see text). The number of Lorentzian peaks used in the fitting was chosen to capture as much of the fermionic resonances as detectable without over-constraining the model. ULE transmission resonances (orange, bottom), obtained simultaneously using the electro-optically modulated fundamental laser light, generate calibration frequency markers for the frequency-doubled light used in spectroscopy.

of interest is larger than the isotope shifts we seek to measure. In order to resolve these shifts, we employ saturated absorption spectroscopy. Light from the SHG stage is sent to our saturated-absorption spectroscopy setup, where the beam is split into a pump with intensity near the saturation intensity I_{sat} (between 0.1 and $15\,\text{mW/mm}^2$ depending on the transition) and a weak (around $I_{\text{sat}}/50$) probe beam. The absorption signal, which is modulated by chopping the pump beam at 6 kHz using an optical chopper wheel, is then demodulated using a lock-in detector, allowing us to extract a clear Doppler-free absorption signal.

In a typical spectrum (Fig. 3), three peaks are evident, corresponding to the three naturally abundant bosonic isotopes. The relative peak amplitudes qualitatively follow the expected isotopic abundance (Table I). The measured isotope shifts for these isotopes are presented in Table II in the Appendix.

Since the two stable fermionic isotopes (^{47}Ti and ^{49}Ti) have nonzero nuclear spin and low natural abundance, their already weak resonances are further split between several hyperfine structure transitions [13,20,28,29]. Therefore, we are unable to isolate the optical resonances and record isotope shifts for these isotopes. The observed Doppler-free linewidths in the lamp are broader than the natural linewidths by approximately 60 MHz, arising primarily due to collisions between the metastable titanium and buffer gas in the HCL, which shortens the lifetime of the excited states [24,30]. Atomic resonances in an HCL are known to suffer from pressure broadening and pressure shifts. Research suggests [31–34] that pressure shifts are smaller than pressure broadening and that systematic changes to the isotopic shifts, which are differential in nature, are well below the sensitivity of our measurement. This, in addition to the fact that our fitting model deviates most strongly from the experimental data in regions where fermionic peaks would be expected, causes us to suspect that trace absorption peaks from the fermions are present but outside the sensitivity of our measurement.

An additional feature, consisting of a broader Gaussian background superimposed on the atomic resonances, is evident. This feature is likely due to diffusion of excited-state atoms, consistent with theoretical models [30] that suggest velocity-changing collisions between the buffer gas and the excited titanium atoms destroy the Doppler-free character of the saturated-absorption measurement scheme for the atoms that undergo collisions. In our system, the mean excited state lifetime of 15 ns is large enough compared to the mean time between collisions of about 150 ns that there is a non-negligible probability that an atom will fall out of the Doppler-free scheme and contribute to this feature.

By fitting the spectra with a physically motivated model that includes all of these features, we can extract the locations of each of the bosonic resonance features, from which we can calculate the isotope shifts.

III. ISOTOPE SHIFT ANALYSIS

The isotope shifts (between isotopes i and j) $d\nu_{ij}$ for a transition can also be decomposed into a normal mass shift $d\nu_{ij}^{\text{NMS}}$, a specific mass shift $d\nu_{ij}^{\text{SMS}}$, and a field shift $d\nu_{ij}^{\text{FS}}$ [1,14,20,35–38] as

$$d\nu_{ij} = d\nu_{ij}^{\text{NMS}} + d\nu_{ij}^{\text{SMS}} + d\nu_{ij}^{\text{FS}}. \tag{1}$$

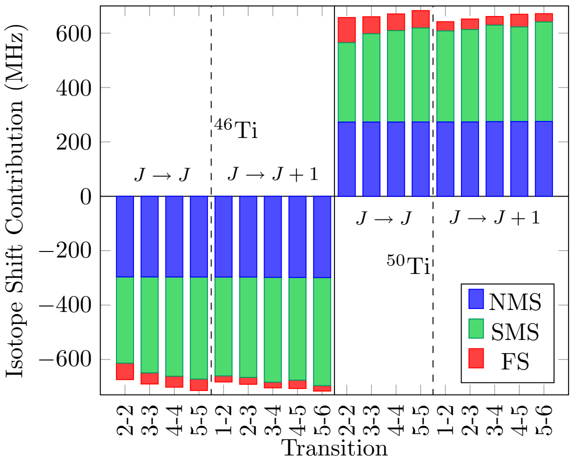

FIG. 4. The contributions to the overall isotope shifts due to the normal mass shift (NMS, blue), specific mass shift (SMS, green), and field shift (FS, red) for ^{46}Ti and ^{50}Ti, relative to ^{48}Ti. The contributions sum to the total isotope shift. The horizontal axis labels are the (J-J') pairs that define the transitions.

The mass shifts both arise from variation in the reduced mass of the electron in the atomic center of mass frame, with the normal mass shift quantifying the change in kinetic energy of individual electrons and the specific mass shift measuring an energy term coming from two-electron momentum correlations. The field shift is due to the difference in charge density of the nucleus between the isotopes. The normal mass shift is readily calculated, and the specific mass and field shifts can be written in terms of specific mass shift and field shift coefficients k_{SMS} and F [1,14,35–39], respectively, such that Eq. (1) reads as

$$d\nu_{ij} = (k_{\text{SMS}} + \nu m_e)\frac{m_i - m_j}{m_i m_j} + F\, d\langle r^2\rangle_{ij} \tag{2}$$

for isotopic masses m_i and m_j, electron mass m_e, optical transition frequency ν, and difference in mean square nuclear charge radii $d\langle r^2\rangle_{ij}$. Defining $\mu_{ij} = m_i m_j/(m_i - m_j)$ such that

$$\mu_{ij} d\nu_{ij} - \nu m_e = k_{\text{SMS}} + F\mu_{ij}\, d\langle r^2\rangle_{ij}, \tag{3}$$

we can determine k_{SMS} and F, given our experimental data and $d\langle r^2\rangle_{ij}$, which are available for titanium from muonic x-ray transition [40] measurements in neutral titanium and collinear laser spectroscopy [36] measurements in the Ti$^+$ ion. The specific mass shift and field shift coefficients calculated from our data are presented in Table IV.

The values of k_{SMS} and F can be used to calculate the contributions of the specific mass shift and the field shift to the total isotopic line shift. These, along with the calculated normal mass shift, are presented together in Table III and Fig. 4. The majority of the fractional error in these values comes from the several-percent uncertainty in the available literature values of $d\langle r^2\rangle_{ij}$ [36,40].

The specific mass shift is larger than the normal mass shift in all the cases examined in this work, as expected for an atom like titanium with many valence electrons [18,20,37,38]. The field shift is weak compared to the mass shifts. Since F is

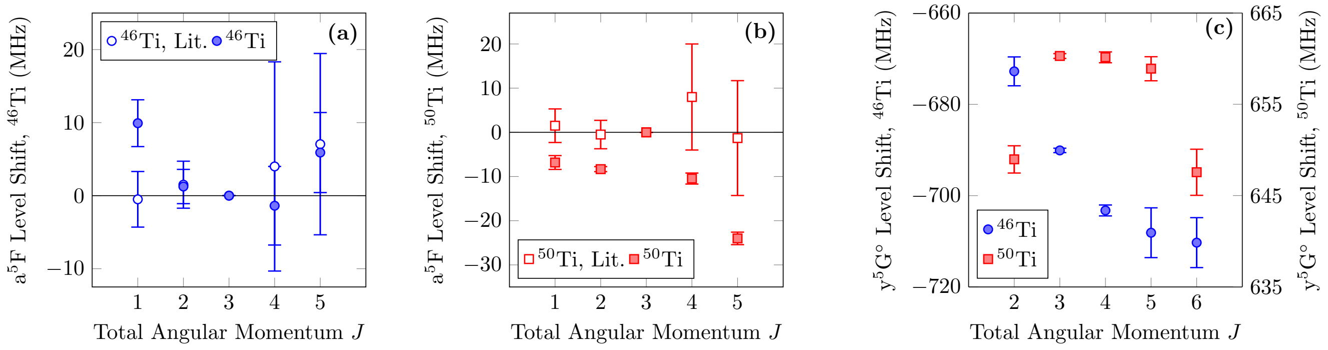

FIG. 5. Isotopic level shifts of the a^5F manifold [panels (a) and (b)] and the y^5G^o manifold [panel (c)] for ^{46}Ti (blue circles) and ^{50}Ti (red squares), relative to the a^5F_3 level. Literature values [14] (open symbols) are plotted where known.

negative, and since $\langle r^2\rangle$ decreases with the addition of neutrons toward the cusp at the magic ^{50}Ti nucleus [20–22], the field shift contributes in the same direction as the mass shifts.

Since the isotope shift is actually a difference of isotopic level shifts, these isotope shift measurements can also be used to calculate all the level shifts for the a^5F and y^5G^o manifolds, relative to some level, provided the isotope shift on enough lines is measured. By measuring the isotope shift on all five $J \rightarrow J+1$ transitions and all four $J \rightarrow J$ transitions, we construct a "ladder" structure (Fig. 1) in which we can, by defining one level to have zero isotopic level shift, determine the level shifts of all of the other levels in the two manifolds. We select the a^5F_3 level as our reference level, since its central location in the a^5F manifold allows us to minimize compounding uncertainty. The level shifts are reported, along with literature values calculated using a similar three-manifold "ladder" [14] where known, in Table IV and Fig. 5. The level shifts reported here improve upon the precision of literature values by a notable margin and agree to within a 95% confidence interval.

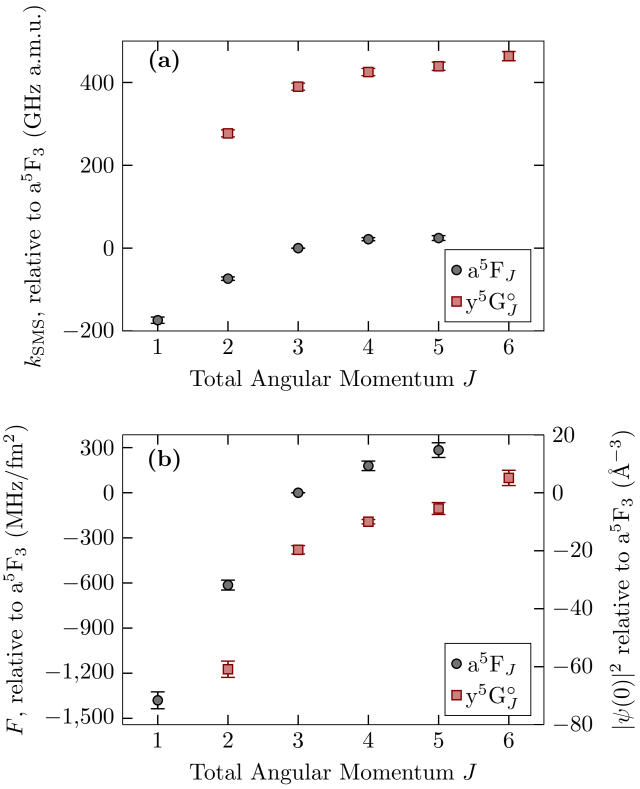

FIG. 6. The (a) specific mass shift and (b) field shift coefficients for the 10 levels investigated, reported relative to a^5F_3. The value of F is proportional to the electron density at the nucleus [(b), right axis].

A similar ladder scheme can be used to calculate the specific mass and field shift coefficients on each level in the two manifolds. From this, the electron density at the nucleus (relative to the a^5F_3 level) can be evaluated [1,3–5].

The values obtained from this analysis, shown in Fig. 6, represent the most significant findings in our work: We observe a clear, monotonic dependence with J in both the specific mass shift and the field shift, for both the metastable a^5F and y^5G^o levels. The variation in $k_{\rm SMS}$ reflects a J-dependent change in the correlated motion of electrons. It is compelling to compare the specific mass shift determined from our measurement with theoretically derived electronic wave functions for atomic titanium.

Variation in the field shift is more straightforwardly related to a specific physical quantity, namely the electron density at the location of the nucleus. We observe that excitation from the metastable a^5F_J levels to the excited $y^5G^o_J$ levels generally lowers the electron density at the nucleus, a trend that is expected since such excitations imply the promotion of a 4s electron into the 4p orbital. Further, in both manifolds, the electron density shows a strong and clear J dependence. In fact, the J-dependent variation of the electron density within each term is far greater than the average difference (about 20 Å^{-3}) between the two terms. This comparison demonstrates the strong electron-correlation effects within the partially filled shells of the titanium atom, and their consequent influence on electronic shielding of the nuclear Coulomb potential.

TABLE I. The five naturally abundant isotopes of titanium [28,29]. The three bosonic isotopes (^{46}Ti, ^{48}Ti, and ^{50}Ti) all have zero nuclear spin, and therefore no hyperfine structure. All five isotopes have more than 5% natural abundance.

Isotope	Nuclear spin	Abundance
^{46}Ti	0	8.25%
^{47}Ti	5/2	7.44%
^{48}Ti	0	73.72%
^{49}Ti	7/2	5.41%
^{50}Ti	0	5.18%

IV. CONCLUSION

In conclusion, we measure and report the isotope shifts in the nine $a^5F_J \rightarrow y^5G^o_{J,J+1}$ transitions in bosonic titanium by performing saturated absorption spectroscopy in a hollow cathode lamp. We use these data to determine the normal mass shift, specific mass shift, and field shift for each stable bosonic isotope and each line. We additionally calculate the isotopic level shifts of all ten levels in the a^5F and y^5G^o energy terms, relative to the a^5F_3 state. We observe a clear and monotonic variation with J both in the specific mass shift and also in the electron density at the nucleus, for both energy terms examined in this work. As such, our work provides a strong complement to prior studies of isotope shifts in atomic fine structure, where the atoms and levels examined showed a more complicated J dependence. Our measurements provide strong benchmarks for theoretical examinations of atomic structure in transition metals. Additionally, by characterizing isotope shifts in transitions suited for laser cooling of atomic titanium, we open the door to studies of ultracold titanium gases.

ACKNOWLEDGMENTS

We thank D. Peña, M. Aguirre, D. Novoa, H. Hu, S. Huber, J. Zeiher, J. Gerber, E. Deist, and J. Isaacs for many helpful discussions over the course of this project. We acknowledge support from the Heising-Simons Foundation, from the ARO (Contracts No. W911NF1910017 and No. W911NF2010266, and through the MURI program with Grant No. W911NF-17-1-0323), and from the California Institute for Quantum Entanglement supported by the Multicampus Research Programs and Initiative of the UC Office of the President (Grant No. MRP-19-601445).

APPENDIX

In this Appendix, we tabulate the numerical data that are discussed in the main body of the paper. Table I lists the stable isotopes of titanium and their nuclear spins. Table II lists the measured value of the isotope shifts for all of the measured transitions, as well as the King parameters. It should be noted that we have provided statistical and systematic error bars for the quantities listed except for one large systematic error due to the uncertainty in measurements of the radii of titanium's nucleus, which leads to a large uncertainty in the field shift coefficients F and any quantities derived from it. A more precise measurement of $d\langle r^2\rangle$ would greatly reduce our systematic uncertainties. Table III lists the breakdown of each transition into the normal mass shift (NMS), specific mass shift (SMS), and the field shift (FS), as shown in Fig. 4. The systematic uncertainty in the nuclear radius also applies to the breakdown between the SMS and FS; we only list the statistical uncertainty of our measurement. Table IV lists the measured isotope shift of each atomic level relative to the a^5F_3 level, as well as the literature values of these level shifts, where available [14].

TABLE II. The isotope shifts, specific mass shift coefficients, and field shift coefficients for the nine strongest transitions between a^5F and y^5G^o. There is a systematic uncertainty in the field and mass shift coefficients arising from uncertainty in literature values [36,40] of $d\langle r^2\rangle_{ij}$, which have several percent standard fractional error. This manifests as a constant 7.37% fractional error on the value of F which propagates into the error on k_{SMS}. For k_{SMS}, the statistical error is reflected in the first of the two error bounds and this systematic error is reflected in the second, and for F, only the statistical error is reported. Shifts are reported as detunings from the ^{48}Ti resonance feature.

Lower	Upper	^{46}Ti shift (MHz)	^{50}Ti shift (MHz)	k_{SMS} (GHz a.m.u.)	F (MHz/fm^2)
a^5F_1	$y^5G^o_2$	−682.69(31)	642.14(38)	401.36(18)(230)	−206.38(14)
a^5F_2	$y^5G^o_2$	−674.0 (22)	657.3 (14)	350.3(12)(63)	−559.6(21)
a^5F_2	$y^5G^o_3$	−691.3 (23)	651.96(50)	407.5(14)(22)	−234.74(80)
a^5F_3	$y^5G^o_3$	−690.09(47)	660.29(28)	389.29(27)(416)	−379.33(30)
a^5F_3	$y^5G^o_4$	−703.2 (12)	660.15(62)	425.72(72)(202)	−192.46(37)
a^5F_4	$y^5G^o_4$	−701.9 (52)	670.6 (11)	403.2(30)(39)	−372.6(28)
a^5F_4	$y^5G^o_5$	−706.74(88)	669.36(39)	417.15(52)(354)	−283.83(39)
a^5F_5	$y^5G^o_5$	−714.02(56)	682.91(56)	414.37(33)(225)	−388.33(44)
a^5F_5	$y^5G^o_6$	−716.19(39)	671.6 (21)	438.77(25)(202)	−185.89(58)

TABLE III. The components of the isotope shifts of bosonic titanium, relative to ^{48}Ti. All shifts in MHz.

Lower	Upper	^{46}Ti $d\nu^{\mathrm{NMS}}$	^{46}Ti $d\nu^{\mathrm{SMS}}$	^{46}Ti $d\nu^{\mathrm{FS}}$	^{50}Ti $d\nu^{\mathrm{NMS}}$	^{50}Ti $d\nu^{\mathrm{SMS}}$	^{50}Ti $d\nu^{\mathrm{FS}}$
a^5F_1	$y^5G^o_2$	−297.0	−363.5(21)	−22.3(21)	273.3	334.7(30)	34.1(30)
a^5F_2	$y^5G^o_2$	−296.4	−317.3(58)	−60.4(58)	272.7	292.1(85)	92.3(85)
a^5F_2	$y^5G^o_3$	−297.4	−369.1(23)	−25.4(23)	273.6	339.8(34)	38.7(34)
a^5F_3	$y^5G^o_3$	−296.5	−352.7(38)	−41.0(38)	272.8	324.8(55)	62.6(55)
a^5F_3	$y^5G^o_4$	−297.9	−385.5(19)	−20.8(19)	274.1	355.0(28)	31.8(28)
a^5F_4	$y^5G^o_4$	−296.7	−365.1(44)	−40.1(44)	272.9	336.2(65)	61.3(65)
a^5F_4	$y^5G^o_5$	−298.4	−377.8(32)	−30.6(32)	274.5	347.8(47)	46.8(47)
a^5F_5	$y^5G^o_5$	−296.9	−375.2(21)	−41.9(21)	273.1	345.5(30)	64.1(30)
a^5F_5	$y^5G^o_6$	−299.0	−397.4(18)	−20.0(18)	275.0	365.9(27)	30.5(27)

TABLE IV. The experimental and literature [14] (where known) isotopic level shifts of the levels in the a^5F and y^5G^o manifolds, relative to a^5F_3. All shifts in MHz.

Level	Level shift, ^{46}Ti	Level shift, ^{50}Ti	Literature level shift, ^{46}Ti	Literature level shift, ^{50}Ti
a^5F_1	9.9(32)	−6.8(16)	−0.5(38)	1.5(38)
a^5F_2	1.3(23)	−8.33(57)	1.5(32)	−0.5(33)
a^5F_3	0.	0.	0.	0.
a^5F_4	−1.4(49)	−10.5(12)	4(14)	8(12)
a^5F_5	5.9(55)	−24.0(14)	7(12)	−1(13)
$y^5G^o_2$	−672.7(32)	649.0(15)		
$y^5G^o_3$	−690.09(47)	660.29(28)		
$y^5G^o_4$	−703.2(12)	660.15(62)		
$y^5G^o_5$	−708.1(54)	658.9(13)		
$y^5G^o_6$	−710.3(55)	647.6(25)		

[1] W. H. King, *Isotope Shifts in Atomic Spectra* (Plenum Press, New York, 1984).

[2] S. Liu and G. Parr, Atomic correlation energy from the electron density at the nucleus, J. Phys. Chem. A **111**, 10422 (2007).

[3] P. Brix and H. Kopfermann, Zur Isotopieverschiebung im Spektrum des Samariums, Z. Phys. **126**, 344 (1949).

[4] A. R. Bodmer, Nuclear scattering of electrons and isotope shift, Proc. Phys. Soc. London, Sect. A **66**, 1041 (1953).

[5] C. Shi, F. Gebert, C. Gorges, S. Kaufmann, W. Nörtershäuser, A. Sahoo, B. K. Surzhykov, V. Yerokhin, J. Berengut, F. Wolf, J. Heip, and P. Schmidt, Unexpectedly large difference of the electron density at the nucleus in the $4p^2P_{1/2,3/2}$ fine-structure doublet of Ca$^+$, in *Exploring the World with the Laser* (Springer, Cham, 2018), Chap. 1, pp. 1–19.

[6] R. F. G. Ruiz, M. L. Bissell, K. Blaum, A. Ekström, N. Frömmgen, G. Hagen, M. Hammen, K. Gebeler, J. D. Holt, G. R. Jensen, M. Kowalska, K. Kreim, W. Nazarewicz, R. Neugart, G. Neyens, W. Mörtershäuser, T. Papenbrock, J. Papuga, A. Schwenk, J. Simonis, K. A. Wendt, and D. T. Yordanov, Unexpectedly large charge radii of neutron-rich calcium isotopes, Nat. Phys. **12**, 594 (2018).

[7] B. K. Sahoo, A. R. Vernon, R. F. G. Ruiz, C. L. Binnersley, J. Billowes, M. L. Bissell, T. E. Cocolios, G. J. Farooq-Smith, K. T. Flanagan, W. Gins, R. P. de Groote, A. Koszorús, G. Neyens, K. M. Lynch, F. Parnefjord-Gustafsson, C. M. Ricketts, K. D. A. Wendt, S. G. Wilkins, and X. F. Yang, Analytic response relativistic coupled-cluster theory: The first application to indium isotope shifts, New J. Phys. **22**, 012001 (2020).

[8] V. V. Flambaum, A. J. Geddes, and A. V. Viatkina, Isotope shift, nonlinearity of King plots, and the search for new particles, Phys. Rev. A **97**, 032510 (2018).

[9] J. C. Berengut, D. Budker, C. Delaunay, V. V. Flambaum, C. Frugiuele, E. Fuchs, C. Grojean, R. Harnik, R. Ozeri, G. Perez, and Y. Soreq, Probing New Long-Range Interactions by Isotope Shift Spectroscopy, Phys. Rev. Lett. **120**, 091801 (2018).

[10] S. Eustice, K. Cassella, and D. Stamper-Kurn, Laser cooling of transition metal atoms, Phys. Rev. A **102**, 053327 (2020).

[11] R. E. S. Clegg, D. L. Lambert, and R. A. Bell, Isotopes of titanium in cool stars, Astrophys. J. **234**, 188 (1979).

[12] Y. V. Pavlenko, S. N. Yurchenko, L. K. McKemmish, and J. Tennyson, Analysis of the TiO isotopologues in stellar optical spectra, Astron. Astrophys. **642**, A77 (2020).

[13] E. M. Azaroual, P. Luc, and R. Vetter, Realization and characterization of a beam of titanium atoms, J. Phys. III (France) **2**, 899 (1992).

[14] S. Kobayashi, N. Nishimiya, and M. Suzuki, Isotope shifts in the spectrum of the neutral titanium atom, Spectrochim. Acta B **152**, 30 (2019).

[15] E. M. Azaroual, P. Luc, and R. Vetter, Isotope shift measurements in titanium I, Z. Phys. D **24**, 161 (1992).

[16] B. Furmann, D. Stefańska, A. Krzykowski, A. Jarosz, and A. Kajoch, Isotope shift in titanium atom, Z. Phys. D **37**, 289 (1996).

[17] P. Luc, R. Vetter, C. Bauche-Arnoult, and J. Bauche, Isotope shift and hyperfine structure measurements in titanium I, Z. Phys. D **31**, 145 (1994).

[18] Y. P. Gangrsky, K. P. Marinova, and S. G. Zemlyanoi, *J* dependences of the isotope shifts in Ti I $3d^24s^2a^3p$ and $3d^34py^3d^\circ$ terms, J. Phys. B: At. Mol. Opt. Phys. **28**, 957 (1995).

[19] A. Anastassov, Y. P. Gangrsky, K. P. Marinova, B. N. Markov, and S. G. Zemlyanoi, Optical isotope shifts and changes in nuclear charge radii of stable Ti isotopes, Z. Phys. D: At., Mol. Clusters **30**, 275 (1994).

[20] W.-G. Jin, Y. Nemoto, and T. Minowa, Hyperfne structure and isotope shift in Ti I by UV laser spectroscopy, J. Phys. Soc. Jpn. **78**, 094301 (2009).

[21] R. J. Lombard, On the size of light nuclei, EPL **12**, 119 (1990).

[22] I. Angeli and K. P. Marinova, Table of experimental nuclear ground state charge radii: An update, At. Data Nucl. Data Tables **99**, 69 (2013).

[23] J. Bauche and R.-J. Champeau, Recent progress in the theory of atomic isotope shift, Adv. At. Mol. Phys. **12**, 39 (1976).

[24] M. A. Norcia and J. K. Thompson, Simple laser stabilization to the strontium ^{88}Sr transition at 707 nm, Rev. Sci. Instrum. **87**, 023110 (2016).

[25] S. Krins, S. Oppel, N. Huet, J. von Zanthier, and T. Bastin, Isotope shifts and hyperfine structure of the Fe I 372-nm resonance line, Phys. Rev. A **80**, 062508 (2009).

[26] M-Squared Lasers SolsTiS, https://www.m2lasers.com/solstis.html.

[27] Stable Laser Systems, 100-kHz linewidth, 1.5-GHz free spectral range, https://stablelasers.com/fabry-perot-cavities/.

[28] G. T. Seaborg and I. Perlman, Table of isotopes, Rev. Mod. Phys. **20**, 585 (1948).

[29] J. R. de Laeter, J. K. Böhlke, P. de Bièvre, H. Hidaka, H. S. Peiser, K. J. R. Rosman, and P. D. P. Taylor, Atomic weights of the elements. Review 2000, Pure Appl. Chem. **75**, 683 (2003).

[30] P. R. Berman, P. F. Liao, and J. E. Bjorkholm, Theory of saturation spectroscopy including collisional effects, Phys. Rev. A **20**, 2389 (1979).

[31] G. Smith, Collision broadening and shift in the resonance line of calcium, J. Phys. B **5**, 2310 (1972).

[32] U. Dammalapati, I. Norris, and E. Riis, Saturated absorption spectroscopy of calcium in a hollow-cathode lamp, J. Phys. B **42**, 165001 (2009).

[33] D. F. Kimball, D. Clyde, D. Budker, D. Demille, S. J. Freedman, S. Rochester, J. E. Stalnaker, and M. Zolotorev, Collisional perturbation of states in atomic ytterbium by helium and neon, Phys. Rev. A **60**, 1103 (1999).

[34] T. Tanabe, D. Akamatsu, H. Inaba, S. Okubo, T. Kobayashi, M. Yasuda, and F.-L. Hong, A frequency-stabilized light source at 399 nm using an Yb hollow-cathode lamp, Jpn. J. Appl. Phys. **57**, 062501 (2018).

[35] N. Huet, M. Pettens, and T. Bastin, Isotope shifts and hyperfine structure of the laser-cooling Fe I 358-nm line, Phys. Rev. A **92**, 052507 (2015).

[36] Y. P. Gangrsky, K. P. Marinova, S. G. Zemlyanoi, I. D. Moore, J. Billowes, P. Campbell, K. T. Flanagan, D. H. Forest, J. A. R. Griffith, J. Huikari, R. Moore, A. Nieminen, H. Thayer, G. Tungate, and J. Äystö, Nuclear charge radii of neutron deficient titanium isotopes ^{44}Ti and ^{45}Ti, J. Phys. G: Nucl. Part. Phys. **30**, 1089 (2004).

[37] C. F. Fischer and L. Smentek-Mielczarek, MCHF evaluation of the specific mass shift, J. Phys. B: At. Mol. Phys. **16**, 3479 (1983).

[38] L. J. S. Halloran, S. Fostner, E. Paradis, and J. A. Behr, Specific mass shift of potassium $5P_{1/2}$ state, Opt. Commun. **282**, 554 (2009).

[39] W. H. King, Comments on the article: Peculiarities of the isotope shift in the samarium spectrum, J. Opt. Soc. Am. **53**, 638 (1963).

[40] H. D. Wohlfahrt, E. B. Shera, M. V. Hoehn, Y. Yamazaki, and R. M. Steffen, Nuclear charge distributions in $1f_{7/2}$-shell nuclei from muonic x-ray measurements, Phys. Rev. C **23**, 533 (1981).